



Cite this: *Nanoscale*, 2016, **8**, 7978

Transparent megahertz circuits from solution-processed composite thin films†

Xingqiang Liu,^a Da Wan,^a Yun Wu,^b Xiangheng Xiao,^a Shishang Guo,^a Changzhong Jiang,^a Jinchai Li,^a Tangsheng Chen,^b Xiangfeng Duan,^c Zhiyong Fan^d and Lei Liao^{*a}

Solution-processed amorphous oxide semiconductors have attracted considerable interest in large-area transparent electronics. However, due to its relative low carrier mobility ($\sim 10 \text{ cm}^2 \text{ V}^{-1} \text{ s}^{-1}$), the demonstrated circuit performance has been limited to 800 kHz or less. Herein, we report solution-processed high-speed thin-film transistors (TFTs) and integrated circuits with an operation frequency beyond the megahertz region on 4 inch glass. The TFTs can be fabricated from an amorphous indium gallium zinc oxide/single-walled carbon nanotube (a-IGZO/SWNT) composite thin film with high yield and high carrier mobility of $>70 \text{ cm}^2 \text{ V}^{-1} \text{ s}^{-1}$. On-chip microwave measurements demonstrate that these TFTs can deliver an unprecedented operation frequency in solution-processed semiconductors, including an extrinsic cut-off frequency ($f_T = 102 \text{ MHz}$) and a maximum oscillation frequency ($f_{\text{max}} = 122 \text{ MHz}$). Ring oscillators further demonstrated an oscillation frequency of 4.13 MHz, for the first time, realizing megahertz circuit operation from solution-processed semiconductors. Our studies represent an important step toward high-speed solution-processed thin film electronics.

Received 26th January 2016,

Accepted 11th March 2016

DOI: 10.1039/c6nr00602g

www.rsc.org/nanoscale

Introduction

Low-cost fabrication of thin-film transistors (TFTs) on a glass substrate can enable a broad spectrum of applications, including radio-frequency identification tags, display drivers, and a whole new generation of wearable electronics.^{1–3} The conventional amorphous silicon (a-Si) and emerging organic semiconductor based TFTs, in general, suffer from low carrier mobility ($\sim 1 \text{ cm}^2 \text{ V}^{-1} \text{ s}^{-1}$) thus are not suitable for high-frequency applications.^{4–6} Meanwhile, even though poly-silicon TFTs have demonstrated more improved performance than a-Si TFTs and organic TFTs, their performance non-uniformity due to grain boundaries also limits their applications on a large scale.⁷ Conversely, TFTs based on amorphous oxide semiconductors, such as amorphous indium gallium zinc oxide (a-IGZO), are emerging as highly promising

candidates due to a number of facts, such as a desirable electron mobility of $\sim 10 \text{ cm}^2 \text{ V}^{-1} \text{ s}^{-1}$, low cost and scalable fabrication processes including ink-jet printing and the sol-gel method.^{8,9} Their solution compatibility and optical transparency have also opened up new horizons for low-cost printable and transparent electronics.^{10,11} Practically, to achieve high-speed gate driver circuits, uniform and homogeneous semi-conducting layers are required in addition to high carrier transport mobility.^{12–14} Though many previous studies suggested that better performance was obtained by adjusting the oxide matrix, the enhancement is limited.¹⁵ Thus further improving the performance of amorphous metal oxide TFTs is an important task for practical circuit level applications.¹⁶ Typically, making materials into a composite system is a convenient route to produce new materials with multiple advantages over single component building blocks.^{17,18} We have previously demonstrated that incorporation of single-walled carbon nanotubes (SWNTs) into amorphous metal oxides can deliver improved performance, such as enhanced carrier mobility and low TFT threshold voltage.^{19–21} And the amorphous metal oxide/SWNT composite TFTs have been shown to be superior to that of the low-temperature poly-silicon in terms of large-area applications.^{22,23} A majority of our previous studies employed a silicon substrate as a global back gate and silicon oxide as a gate dielectric, which required high gate switching voltage and was unable to independently address multiple devices on the same chip. Top-gated devices using high-*k*

^aDepartment of Physics and Key Laboratory of Artificial Micro- and Nano-structures of Ministry of Education, Wuhan University, Wuhan 430072, China.
E-mail: liaolei@whu.edu.cn

^bScience and Technology on Monolithic Integrated Circuits and Modules Laboratory, Nanjing Electronic Device Institute, Nanjing 210016, China

^cDepartment of Chemistry and Biochemistry, University of California, Los Angeles, CA 90095, USA

^dDepartment of Electronic & Computer Engineering, The Hong Kong University of Science & Technology, Hong Kong SAR, China

†Electronic supplementary information (ESI) available. See DOI: 10.1039/c6nr00602g

dielectrics can significantly impact critical device performance from transconductance, subthreshold swing, and parasitic capacitance to frequency response. And circuit integration with high-performance top-gated composite TFTs would be urgent for practical applications. In fact, implementation of a ring oscillator can be the ultimate test for new materials in high-frequency applications and to evaluate their compatibility with conventional circuit architectures.^{24,25} Herein, we report a high-performance top-gated a-IGZO/SWNT composite TFT using a sol-gel method. In the device configuration, the presence of conductive SWNTs reduces the effective distance between the source and drain, resulting in a reduced effective channel length. The metallic conductive SWNTs supplied fast conductivity tracks at the on state and the a-IGZO pinched off the active channel at the off state.^{24,26,27} This might be the rationale for the enhanced mobility and obtained a higher on-off ratio than the SWCNT devices.²⁸ Based on the improved performance of the single top-gated TFT, three-stage ring oscillators were fabricated on glass with an oscillation frequency of 4.13 MHz, corresponding to a propagation delay of less than 40.3 nanoseconds per stage. To our best knowledge, this recorded speed not only largely surpasses that of the amorphous metal oxide, amorphous silicon and organic based devices,^{29–39} but also reaches the level of poly-silicon devices with a similar geometry (the propagation delay is in the range of several nanoseconds per stage).^{40–42}

Results and discussion

A cross-sectional schematic of the top-gated a-IGZO/SWNT composite TFT on a glass substrate is shown in Fig. 1a. The a-IGZO/SWNT composite thin films were fabricated using a

sol-gel method and the details can be found in the Experimental section. The precursor solutions were prepared using the optimized recipe for comprehensively high performance, and the fabrication method has been demonstrated to be scalable for fabricating high-performance a-IGZO/SWNT composite thin films with small device-device variations.^{19–21} The entire composite film was divided into 10 $\mu\text{m} \times 100 \mu\text{m}$ isolated chips by wet etching for further integration. The top gate area was patterned by e-beam lithography (EBL), and then 30 nm HfO_2 dielectric was deposited by atomic layer deposition (ALD),⁴³ followed by 10 nm/40 nm Cr/Au gate electrode evaporation. Finally, the source/drain electrodes were defined by EBL and metallization processes. The electrical measurements were performed with a LakeShore TTPX probe station and a semiconductor parameter analyzer. The transfer characteristics of the fabricated TFTs show n-type characteristics expected for the oxide matrix (Fig. 1b) and the typical gate current is shown in Fig. S1.† By differentiating the transfer characteristics, the peak transconductance was obtained as 133.3 μS with a low sub-threshold swing of 85 mV dec^{-1} . The field-effect mobility was then calculated to be 74.5 $\text{cm}^2 \text{V}^{-1} \text{s}^{-1}$ by using

$$\mu = \frac{g_m L}{V_{ds} C_i W}$$

where g_m can be obtained by deriving the $I_{ds}-V_g$ curve, L and W are the channel length and width, respectively, and C_i is the insulator capacitance per unit area, and the mobility value is approaching that of the low-temperature poly-silicon TFTs.^{40–42} Fig. 1c shows representative output characteristics of $I_{ds}-V_{ds}$ curves of the a-IGZO/SWNT TFTs. The current saturation at high V_{ds} and the linear characteristics of I_{ds} at low V_{ds} indicate that ohmic-like contacts are formed between the a-IGZO/SWNT thin films and Cr/Au electrodes, and they also suggest that the channel is effectively controlled by the gate potential. The statistical data for the composite TFTs with different channel lengths are shown in Fig. 1d, which represent desirable performance uniformity. Compared with that of the back-gated devices with the same channel materials, which have mobility typically around 120 $\text{cm}^2 \text{V}^{-1} \text{s}^{-1}$, the slightly degraded mobility here may be caused by the thermal and wet surroundings during the ALD procedures and the parasitic resistance from the gap between the gate and source/drain electrodes.⁴⁴

An important benchmark of the transistor radio-frequency performance is the cut-off frequency (f_T) and the maximum oscillation frequency (f_{max}).⁴⁵ To assess the radio-frequency characteristics of the a-IGZO/SWNT composite TFTs, on-chip microwave measurements were carried out in the range of 10–200 MHz with an Agilent N5247A network analyzer using ground-signal-ground probes, as shown in Fig. 2a. Fig. 2b shows the $|h_{21}|$ current gain derived from the measured scattering parameters at $V_g = 2.75 \text{ V}$ and $V_{ds} = 3 \text{ V}$, and the selected V_g value is the peak transconductance point for the device. It has the typical $1/f$ frequency dependence expected for an ideal field-effect transistor, yielding a f_T of 102 MHz. Notably, this

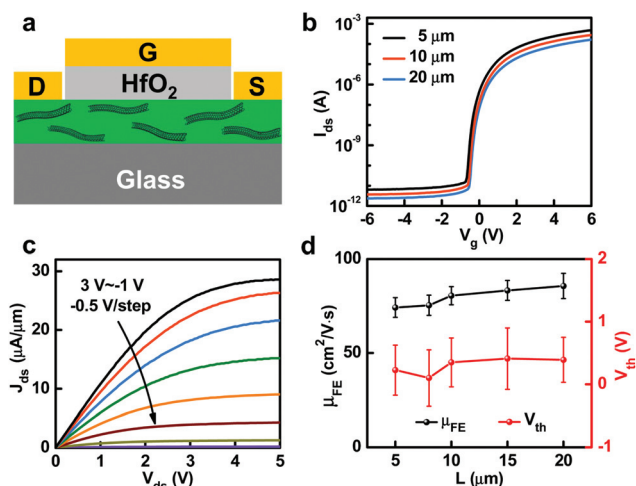


Fig. 1 (a) Schematic of the device layout. D, drain; G, gate; S, source. (b) Transfer characteristics of a-IGZO/SWNT composite TFTs with different channel lengths (L); and the channel width (W) is fixed to be 10 μm . (c) Typical output characteristics of a-IGZO/SWNT composite TFTs with $L = 5 \mu\text{m}$. (d) The plot of mobility and V_{th} versus the channel length. The error bars indicate the standard deviation over 20 devices.

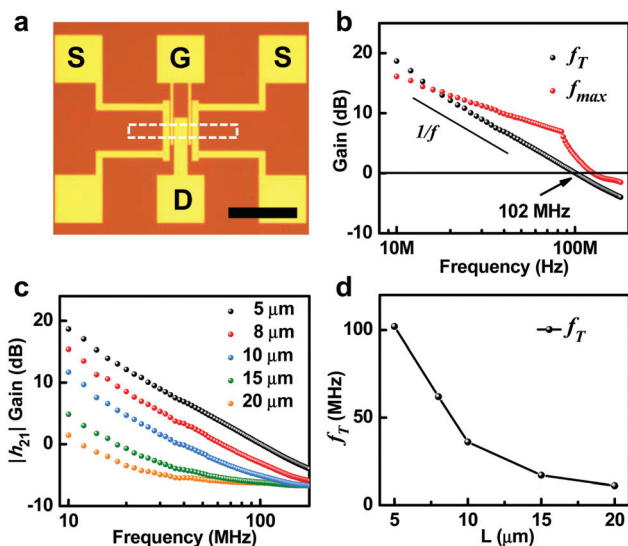


Fig. 2 (a) Micro-graph of the fabricated TFTs with $L/W = 5 \mu\text{m}/10 \mu\text{m}$, and the scale bar is $100 \mu\text{m}$. (b) Measured small-signal current gain $|h_{21}|$ as a function of frequency at $V_{ds} = 2.75 \text{ V}$, $V_g = 3 \text{ V}$; the V_g value used is the peak transconductance point for the device. (c) Small-signal current gain $|h_{21}|$ as a function of frequency with different channel lengths. (d) The plot of f_T as a function of the channel length.

value will fully fulfill the radio-frequency identification tags, in which 13.56 MHz is adopted for 70% of such applications. To obtain the frequency limit of an a-IGZO/SWNT composite TFT, we measured the f_{max} as well, as shown in Fig. 2b, which shows a $f_{max} = 122 \text{ MHz}$. The results presented here are on a par with that of the InZnO TFTs with an even smaller channel length of $1 \mu\text{m}$.^{45–47} Fig. 2c further shows the $|h_{21}|$ current gain results obtained from the channel length varied from $5 \mu\text{m}$ to $20 \mu\text{m}$. And Fig. 2d shows the plot of the f_T versus the channel length, which presents the typical $1/L^2$ frequency dependence.

The primary advantage of fabricating semiconductor thin films *via* a sol-gel approach is its attractive scalability, as shown in Fig. 3a. We have realized large-scale fabrication of a-IGZO/SWNT composite TFTs on a 4 inch glass wafer, as also shown in the inset. A proof-of-concept demonstration of the a-IGZO/SWNT composite TFT logic circuit was implemented by assembling a basic NOT-inverter logic device. Two a-IGZO/SWNT composite TFTs with different L/W ratios were connected in series (inset of Fig. 3b).^{20,39} The transistor with a smaller L/W ratio ($L/W = 5 \mu\text{m}/10 \mu\text{m}$) serves as the switch of the inverter, while that with the larger L/W ratio ($L/W = 50 \mu\text{m}/10 \mu\text{m}$) functions as the load. The logic circuit was completed by connecting the load transistor to the supply voltage (V_{dd}) and the drive transistor to the ground. The connection between the switch and the load acts as the output terminal. As the V_{in} applied to the switch transistor is increased, the switch transistor is turned on, and the channel resistance drops below the resistance of the load transistor. This effect dramatically reduced the V_{out} , *i.e.*, the signal is inverted. Fig. 3b shows the inversion of the a-IGZO/SWNT inverter at

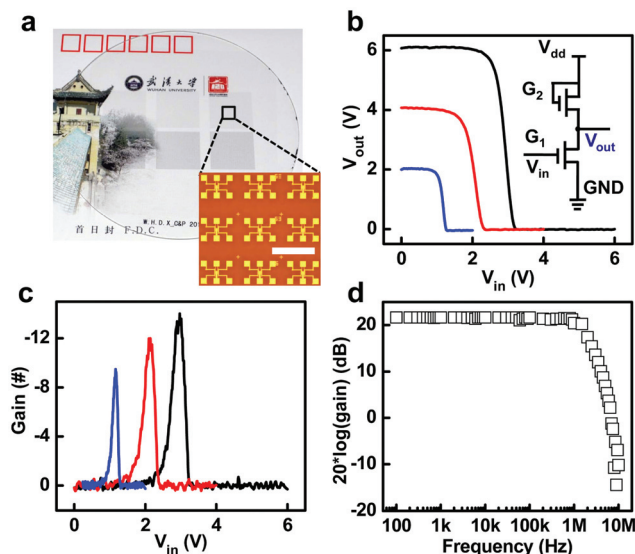


Fig. 3 (a) Optical micro-graphs of an a-IGZO/SWNT inverter on a 4 inch glass substrate; the inset is the TFT array and the scale bar is $500 \mu\text{m}$. (b) The voltage transfer characteristic of an inverter; the inverter is schematically depicted in the inset. (c) DC gain of the a-IGZO/SWNT inverter. (d) AC gain (dB) of the inverter at different frequencies. This inverter shows $f_T > 7 \text{ MHz}$.

different V_{dd} . As V_{dd} varies from 2 to 6 V, the output voltage (V_{out}) remains at the same level as V_{dd} at low V_{in} . As V_{in} is increased, V_{out} promptly dropped to 0 V, and the inverter threshold voltage is measured to be nearly half of the V_{dd} . The calculated signal inverter gain (dV_{out}/dV_{in}) increases with V_{dd} , and the maximum gain value exceeded 14 at $V_{dd} = 6 \text{ V}$ (Fig. 3c), confirming the significant potential of a-IGZO/SWNT composite TFTs for circuit level applications. By measuring the dynamic response of the inverter with a harmonic-waveform input signal from 100 to 10 MHz, as shown in Fig. 3d, it was found that the inverter has a cut-off frequency above 7 MHz. Note that this value is obtained for the TFT with a parasitic resistance in the composite channel, thus limited by the excessive channel length of the load TFT and the parasitic resistance.

The close-to-ideal inverter behavior manifested by the a-IGZO/SWNT integrated circuit enables implementation of a ring oscillator (RO). The propagation delay of the RO is a widely accepted benchmark of how fast the TFTs fabricated under a certain design rule can operate.⁴⁸ Fig. 4a shows the integration process of the three-stage a-IGZO/SWNT RO circuit. The optical micro-graph of the three-stage oscillators is depicted in Fig. 4b. The labels V_{dd} , V_{out} and GND correspond to the supplied voltage, the output voltage and the ground for the ring oscillator, respectively. In the RO, a-IGZO/SWNT inverters are connected in series with an additional inverter connected at the output of the oscillator functioning as a buffer stage. The output signal of the RO was measured as a function of the supply voltage (Fig. 4c). A resonance occurs at 1.60 MHz for $V_{dd} = 4 \text{ V}$, and the improvement in frequency performance with increasing V_{dd} can be attributed to the enhancement in

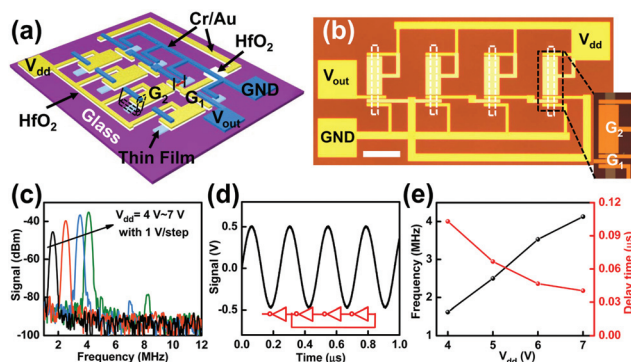


Fig. 4 (a) Schematic illustration of an integrated three-stage ring oscillator circuit on a-IGZO/SWNT composite thin films, which is constructed by integrating 8 a-IGZO/SWNT composite TFTs. The first Cr/Au film is on the HfO₂ as the gate electrode and the second Cr/Au film is in direct contact with the a-IGZO/SWNT composite thin films. The fabricated ring oscillator circuit corresponding to the design above is shown in Fig. 3b. The general aspects of the fabrication process apply to all the devices and logic circuits presented in this paper. (b) Optical micrograph of a three-stage ring oscillator and the scale bar is 50 μm. (c) The power spectrum of the output signal as a function of V_{dd} . The corresponding fundamental oscillation frequency increases from 1.60 MHz to 4.13 MHz. (d) Output voltage as a function of time for the ring oscillator at $V_{dd} = 7$ V. (e) Plots of the maximum oscillation frequency and propagation delay time as a function of the supplied voltage.

the current driving capability of the ring oscillator due to the rise in the drain current I_{ds} in each individual TFT with increasing drain and gate voltages. Between $V_{dd} = 4$ V and $V_{dd} = 7$ V, the signal amplitude measured by the spectrum analyzer changes from -45.6 dBm to -35.2 dBm, again as a consequence of the I_{ds} - V_{dd} dependence. The frequency increases with the voltage and reaches 4.13 MHz at $V_{dd} = 7$ V, with a corresponding stage-delay time of 40.3 nanoseconds, as shown in Fig. 4d. This behavior is a result of the increasing drain current in the individual TFTs with increasing gate/drain voltages, as also shown in Fig. 4e, in which the maximum propagation delay presents nearly a linear relationship with the supplied voltage, and it agrees with the anticipated operation of the ring oscillator. Compared with the previous ROs fabricated with amorphous silicon, organic semiconductors and amorphous metal oxides with a typical oscillation frequency lower than 800 kHz,^{20,35} due to the improved carrier mobility, our RO shows a largely improved frequency response. Moreover, the stage-delay obtained here approaches that of the low-temperature poly-silicon RO.³⁸ Notably, the measured frequencies here are still limited by the parasitic resistance rather than by the intrinsic a-IGZO/SWNT composite.

Experimental

Thin film deposition

The clean glass substrates were treated with oxygen plasma for 5 min. The a-IGZO/SWNT composite thin films were formed

using a spin coating method at a speed of 3000 rpm for 60 s. Then the spin-coated films were pre-baked on the hot plate at 150 °C for 10 min to remove the organic solvent. The spin-coating processes were repeated 3 times to achieve 60 nm composite thin films. The as-prepared thin films were annealed on the hot plate at 250 °C for 40 min under ambient conditions.

Device fabrication

A photolithography and a wet etching process were conducted to divide the fabricated a-IGZO/SWNT composite thin films into 10 μm × 100 μm isolated chips for further integration. Then the top gate area was patterned by EBL. 30 nm ALD of HfO₂ on the contacted a-IGZO/SWNT composite thin films is performed at 95 °C using the KE-MICRO TALD-200A system. The samples were then transferred into the chamber of a metal evaporator for deposition of a 10 nm/40 nm Cr/Au self-aligned gate electrode followed by a lift-off process. Subsequently, a second EBL was used to define the source/drain pattern with the alignment. To avoid the short-circuiting of the gate electrode with the source/drain electrodes, 0.3 μm space margin was designed on both sides of the gate electrode. After metallization of source/drain electrodes and the lift-off process, an individual TFT structure was complete. For ring oscillator fabrication, after the formation of the gate structure, a 30 nm HfO₂ was deposited on the selected area to avoid the short-circuiting between the metal wires.

Measurements

Electrical measurements were performed on the LakeShore TTPX probe station with Keithley 4200 and Keysight B1500A. Characterization of individual a-IGZO/SWNT composite TFTs, as well as the a-IGZO/SWNT inverters were conducted with an Agilent 4155C semiconductor parameter analyzer under an ambient environment. The on-chip microwave measurements were carried out in the 10 MHz–200 MHz range using an Agilent N5247A network analyzer. During the AC measurement of the a-IGZO/SWNT inverters, the input signals were supplied to the circuits with an Agilent 33210A arbitrary waveform generator. Small V_{in-AC} signals of $V_{pp} = 100$ mV with different frequencies on the gate bias as $V_{dd} = 2$ V were applied. And the output waveform signals were recorded by using an Agilent DSO-X2022A digital storage oscilloscope. The output signals of the ring oscillators were measured with an Agilent CXA signal analyzer and an Agilent DSO-X2022A digital storage oscilloscope.

Conclusions

In summary, high-speed devices are fabricated on 4 inch glass substrates using sol-gel processed a-IGZO/SWNT composite thin films as active channel layers. The fabrication process is applicable to a broad range of amorphous metal oxide based composite TFT applications. Ring oscillators have also been implemented showing short propagation delay. The highly attractive transistor performance achieved in the a-IGZO/

SWNT composite devices inspires further development of high-speed functional electronics based on this unique material system.

Acknowledgements

This work was supported by the 973 grant of MOST (No. 2013CBA01604), MOE (20120141110054), NSFC grant (No. 61222402, 61376085, and 61574101), and the key grant of the National Laboratory of Infrared Physics in the Shanghai Institute of Technical Physics (Z201402), as well as GRF 623112 from the Hong Kong Research Grant Council.

Notes and references

- 1 K. Nomura, H. Ohta, A. Takagi, T. Kamiya, M. Hirano and H. Hosono, *Nature*, 2004, **432**, 488.
- 2 K. Nomura, H. Ohta, K. Ueda, T. Kamiya, M. Hirano and H. Hosono, *Science*, 2003, **300**, 1269.
- 3 M. G. Kim, M. G. Kanatzidis, A. Facchetti and T. J. Marks, *Nat. Mater.*, 2011, **10**, 382.
- 4 D. H. Lee, Y. J. Chang, G. S. Herman and C. H. Chang, *Adv. Mater.*, 2007, **19**, 843.
- 5 E. Fortunato, P. Barquinha, G. Goncalves, L. Pereira and R. Martins, *Solid-State Electron.*, 2008, **52**, 443.
- 6 H. Klauk, U. Zschieschang, J. Pflaum and M. Halik, *Nature*, 2007, **445**, 745.
- 7 B. Kumar, B. K. Kaushik and Y. S. Negi, *Polym. Rev.*, 2014, **54**, 33.
- 8 V. Subramanian, J. M. Fréchet, P. C. Chang, D. C. Huang, J. B. Lee, S. E. Molesa, A. R. Murphy, D. R. Redinger and S. K. Volkman, *Proc. IEEE*, 2005, **93**, 1330.
- 9 C. D. Dimitrakopoulos and D. J. Masecaro, *IBM J. Res. Dev.*, 2001, **45**, 11.
- 10 K. Banger, Y. Yamashita, K. Mori, R. Peterson, T. Leedham, J. Rickard and H. Sirringhaus, *Nat. Mater.*, 2011, **10**, 45.
- 11 Y. Wang, X. W. Sun, G. K. L. Goh, H. V. Demir and H. Y. Yu, *IEEE Trans. Electron Devices*, 2011, **58**, 480.
- 12 E. Fortunato, P. Barquinha and R. Martins, *Adv. Mater.*, 2012, **24**, 2945.
- 13 Z. Fan, J. C. Ho, T. Takahashi, R. Yerushalmi, K. Takei, A. C. Ford, Y. L. Chueh and A. Javey, *Adv. Mater.*, 2009, **21**, 3730.
- 14 X. Liu, Y. Z. Long, L. Liao, X. Duan and Z. Fan, *ACS Nano*, 2012, **6**, 1888.
- 15 X. Yu, J. Smith, N. Zhou, L. Zeng, P. Guo, Y. Xia, A. Alvarez, S. Aghion, H. Lin and J. Yu, *Proc. Natl. Acad. Sci. U. S. A.*, 2015, **112**, 3217.
- 16 X. F. Duan, *IEEE Trans. Electron Devices*, 2008, **55**, 3056.
- 17 K. W. Lee, K. Y. Heo, S. H. Oh, A. Moujoud, G. H. Kim and H. J. Kim, *Thin Solid Films*, 2009, **517**, 4011.
- 18 K. W. Lee, K. Y. Heo and H. J. Kim, *Appl. Phys. Lett.*, 2009, **94**, 102112.
- 19 X. Q. Liu, C. L. Wang, X. H. Xiao, J. L. Wang, S. S. Guo, C. Z. Jiang, W. J. Yu, W. D. Hu, J. C. Li and L. Liao, *Appl. Phys. Lett.*, 2013, **103**, 223108.
- 20 X. Q. Liu, W. Liu, X. H. Xiao, C. L. Wang, Z. Y. Fan, Y. Q. Qu, B. Cai, S. S. Guo, J. C. Li, C. Z. Jiang, X. F. Duan and L. Liao, *Nanoscale*, 2013, **5**, 2830.
- 21 X. Q. Liu, C. L. Wang, B. Cai, X. H. Xiao, S. S. Guo, Z. Y. Fan, J. C. Li, X. F. Duan and L. Liao, *Nano Lett.*, 2012, **12**, 3596.
- 22 D. H. Kim, J. H. Ahn, H. S. Kim, K. J. Lee, T. H. Kim, C. J. Yu, R. G. Nuzzo and J. A. Rogers, *IEEE Electron Device Lett.*, 2008, **29**, 73.
- 23 A. Pecora, L. Maiolo, M. Cuscunà, D. Simeone, A. Minotti, L. Mariucci and G. Fortunato, *Solid-State Electron.*, 2008, **52**, 348.
- 24 F. N. Ishikawa, M. Curreli, C. A. Olson, H. I. Liao, R. Sun, R. W. Roberts, R. J. Cote, M. E. Thompson and C. W. Zhou, *ACS Nano*, 2010, **4**, 6914.
- 25 L. Liao, Y. C. Lin, M. Bao, R. Cheng, J. Bai, Y. Liu, Y. Qu, K. L. Wang, Y. Huang and X. Duan, *Nature*, 2010, **467**, 305.
- 26 M. Steiner, M. Engel, Y. M. Lin, Y. Wu, K. Jenkins, D. B. Farmer, J. J. Humes, N. L. Yoder, J. W. T. Seo and A. A. Green, *Appl. Phys. Lett.*, 2012, **101**, 053123.
- 27 Z. Chen, J. Appenzeller, Y. M. Lin, J. Sippel-Oakley, A. G. Rinzler, J. Tang, S. J. Wind, P. M. Solomon and P. Avouris, *Science*, 2006, **311**, 1735.
- 28 X. Z. Bo, N. Tassi, C. Lee, M. Strano, C. Nuckolls and G. B. Blanchet, *Appl. Phys. Lett.*, 2005, **87**, 203510.
- 29 D. A. Mourey, D. A. Zhao, J. Sun and T. N. Jackson, *IEEE Trans. Electron Devices*, 2010, **57**, 530.
- 30 J. Boyce, R. Fulks, J. Ho, R. Lau, J. Lu, P. Mei, R. Street, K. Van Schuylenbergh and Y. Wang, *Thin Solid Films*, 2001, **383**, 137.
- 31 K. Cherenack, B. Hekmatshoar, J. C. Sturm and S. Wagner, *IEEE Trans. Electron Devices*, 2010, **57**, 2381.
- 32 B. Crone, A. Dodabalapur, R. Sarpeshkar, R. Filas, Y. Y. Lin, Z. Bao, J. O'Neill, W. Li and H. Katz, *J. Appl. Phys.*, 2001, **89**, 5125.
- 33 N. Kang, B. K. Sarker and S. I. Khondaker, *Appl. Phys. Lett.*, 2012, **101**, 233302.
- 34 N. A. Azarova, J. W. Owen, C. A. McLellan, M. A. Grimminger, E. K. Chapman, J. E. Anthony and O. D. Jurchescu, *Org. Electron.*, 2010, **11**, 1960.
- 35 M. Ofuji, K. Abe, H. Shimizu, N. Kaji, R. Hayashi, M. Sano, H. Kumomi, K. Nomura, T. Kamiya and H. Hosono, *IEEE Electron Device Lett.*, 2007, **28**, 273.
- 36 T. Sekitani, U. Zschieschang, H. Klauk and T. Someya, *Nat. Mater.*, 2010, **9**, 1015.
- 37 W. Fix, A. Ullmann, J. Ficker and W. Clemens, *Appl. Phys. Lett.*, 2002, **81**, 1735.
- 38 M. N. Troccoli, A. J. Roudbari, T. K. Chuang and M. K. Hatalis, *Solid-State Electron.*, 2006, **50**, 1080.
- 39 Y. Yuan, G. Giri, A. L. Ayzner, A. P. Zoombelt, S. C. B. Mannsfeld, J. Chen, D. Nordlund, M. F. Toney, J. Huang and Z. Bao, *Nat. Commun.*, 2014, **5**, 4005.

- 40 Y. J. Chen, Y. J. Lee and Y. H. Yu, *IEEE Trans. Microwave Theory Tech.*, 2010, **58**, 3444.
- 41 I. Brunets, J. Holleman, A. Y. Kovalgin, A. Boogaard and J. Schmitz, *IEEE Trans. Electron Devices*, 2009, **56**, 1637.
- 42 Y. L. Wang, L. Covert, T. Anderson, W. Lim, J. Lin, S. Pearton, D. Norton, J. Zavada and F. Ren, *Electrochem. Solid-State Lett.*, 2008, **11**, H60.
- 43 X. Zou, J. Wang, C. H. Chiu, Y. Wu, X. Xiao, C. Jiang, W. W. Wu, L. Mai, T. Chen and J. Li, *Adv. Mater.*, 2014, **26**, 6255.
- 44 Y. H. Kim, J. S. Heo, T. H. Kim, S. Park, M. H. Yoon, J. Kim, M. S. Oh, G. R. Yi, Y. Y. Noh and S. K. Park, *Nature*, 2012, **489**, 128.
- 45 H. Chen, Y. Cao, J. Zhang and C. Zhou, *Nat. Commun.*, 2014, **5**, 4097.
- 46 Y. H. Kim, J. S. Heo, T. H. Kim, S. Park, M. H. Yoon, J. Kim, M. S. Oh, G. R. Yi, Y. Y. Noh and S. K. Park, *Nature*, 2012, **489**, 128.
- 47 L. Y. Su and J. Huang, *Solid-State Electron.*, 2015, **104**, 122.
- 48 X. F. Duan, C. Niu, V. Sahi, J. Chen, J. W. Parce, S. Empedocles and J. L. Goldman, *Nature*, 2003, **425**, 274.